different pairs of atoms comprise 23 different distance types (which may be identified by reference to the numbering scheme shown in Fig. 3 and to the list in Table 1). The structure was refined by least-squares fitting of a theoretical intensity curve to those observed (*13*); the parameters adjusted were the two structure-defining radii and 18 vibrational amplitudes (including three groups indicated by the bracketed quantities of Table 1). To be able to refine such a large number of amplitudes is unusual; it owes to the high number ratio of interatomic distance to structure-specifying parameters.

The type of distance consistent with the electron-scattering equations is $r_a$. Owing to the effects of vibration, neither $r_a$ nor the physically more meaningful thermal average distance $r_g$ (*14*) is consistent with equilibrium molecular symmetry. Imposition of symmetry on an $r_a$ distance set will thus lead to compromises in the fit. The distance values obtained for stiff molecules under these circumstances usually do not differ more than a few thousands of an angstrom from those that would be obtained without symmetry restriction. For $C_{60}$, imposition of icosahedral symmetry on the $r_a$ distances seems to have been an excellent assumption, judged by the nearly level character of the difference (residual) curves (Figs. 1 and 2).

The thermal average ($r_g$) bond lengths are expected to be about 0.003 to 0.005 Å longer than the equilibrium values, but their difference should be nearly the same as the $r_e$ (equilibrium) difference. The thermal average bond length should also be longer than the distances in the crystal when the latter are not corrected for thermal motion, both because of the temperature difference between the two experiments, and because distances in the crystal are calculated from determinations of atomic positions. Although there are no values for $C_{60}$ itself, there are x-ray measurements for an osmylated $C_{60}$: Average values are $r(C_1–C_2)$ = 1.423(5) Å and $r(C_1–C_6)$ = 1.388(9) Å (*15*). Our bond lengths are in good agreement with the NMR values (*1*). In principle, the results from these two experiments should differ, both because of the great experimental temperature difference and because the $r$ values retrieved from them have different definitions (electron diffraction: $\langle r \rangle$; NMR: $\langle 1/r^3 \rangle^{-1/3}$). The uncertainties on the values, however, are larger than the expected difference.

The measured root-mean-square amplitudes of vibration ($l$) reveal $C_{60}$ to be a very stiff molecule relative to usual standards. For example, the longest distances in the molecule, that is, those between atoms on opposite sides of the sphere, have associated amplitudes only slightly greater than are found for some of the distances in much smaller molecules at room temperature. As expected, the bond amplitudes are somewhat larger than would be expected for this type of structure at room temperature, but whether the increase is consistent with the temperature of our experiment cannot be judged without appropriate normal-coordinate analysis.

REFERENCES AND NOTES


1. C. S. Yannoni, P. P. Bernier, D. S. Bethune, G. Meijer, J. R. Salem, *J. Am. Chem. Soc.* **113**, 3190 (1991).
2. F. Li, D. Ramage, J. S. Lannin, J. Conceicao, private communication.
3. D. M. Cox *et al.*, *Mater. Res. Soc. Symp. Proc.* **206**, in press.
4. M. Haeser, J. Almlöf, G. E. Scuseria, *Chem. Phys. Lett.* **181**, 497 (1991).
5. W. Kratschmer, L. D. Lamb, K. Fostiropoulos, D. R. Huffman, *Nature* **347**, 354 (1990).
6. R. E. Haufler *et al.*, *J. Phys. Chem.* **94**, 8634 (1990).
7. R. Taylor, J. P. Hare, A. K. Abdul-Sada, H. W. Kroto, *Chem. Comm.*, 1423 (1990).
8. R. D. Johnson, G. Meijer, D. S. Bethune, *J. Am. Chem. Soc.* **113**, 8983 (1990).
9. H. Ajie *et al.*, *J. Phys. Chem.* **94**, 8630 (1990).
10. C. Pan, M. P. Sampson, Y. Chai, R. H. Hauge, J. L. Margrave, *ibid.* **95**, 2944 (1991).
11. Unlike most substances we have studied, the scattering was barely visible on the fluorescent screen and the ambient pressure in the apparatus (about $4 \times 10^{-6}$ Torr) remained unchanged upon opening and closing the oven valve. That diffraction photographs were obtained under such conditions owes to the extremely high scattering power of molecules of $C_{60}$ arising from the high multiplicity of the different distances.
12. G. Gundersen and K. Hedberg, *J. Chem. Phys.* **51**, 2500 (1965); L. Hedberg, paper T9 presented at the Fifth Austin Symposium on Gas-Phase Molecular Structure, Austin, TX, March 1974.
13. K. Hedberg and M. Iwasaki, *Acta Crystallogr.* **17**, 529 (1964).
14. The distance types are related by $r_a = r_g - l^2/r$, where $l$ is the root-mean-square amplitude of vibration of the atomic pair.
15. J. M. Hawkins, A. Meyer, T. A. Lewis, S. Loren, F. J. Hollander, *Science* **252**, 312 (1991).


16. This work was supported in part by the National Science Foundation under grant CHE88-10070 to Oregon State University. We are most grateful to O. Chapa-Perez, who made technical contributions to the IBM work, and to R. Boyer, J. Archibald and G. Allison of Oregon State, who built the high-temperature nozzle-oven.

6 August 1991; accepted 13 September 1991


# The First Step in Vision: Femtosecond Isomerization of Rhodopsin


R. W. SCHOENLEIN, L. A. PETEANU, R. A. MATHIES, C. V. SHANK



**The kinetics of the primary event in vision have been resolved with the use of femtosecond optical measurement techniques. The 11-*cis* retinal prosthetic group of rhodopsin is excited with a 35-femtosecond pump pulse at 500 nanometers, and the transient changes in absorption are measured between 450 and 580 nanometers with a 10-femtosecond probe pulse. Within 200 femtoseconds, an increased absorption is observed between 540 and 580 nanometers, indicating the formation of photoproduct on this time scale. These measurements demonstrate that the first step in vision, the 11-*cis*→11-*trans* torsional isomerization of the rhodopsin chromophore, is essentially complete in only 200 femtoseconds.**


LIGHT DETECTION BY THE VISUAL system is one of nature's most important information transduction processes. It consists of a series of chemical reactions that are initiated by the absorption of a photon and culminate in the stimulation of the optic nerve. It has long been known that the primary step in vision is the photoisomerization of the retinal chromophore in rhodopsin (*1*). However, understanding the dynamics of this isomerization remains a fundamental problem in photochemistry and biology. The time course of many photochemical reactions can be studied with compressed femtosecond optical pulses (*2*). Such pulses were previously used to observe the isomerization of the retinal chromophore in bacteriorhodopsin, a related pigment which functions as a light-driven proton pump (*3*). Recent advances in the generation of femtosecond pulses in the blue-green spectral region now make it possible to study a much wider range of ultrafast processes with a time resolution of 10 fs (*4*). We report here the room temperature investigation of the *cis-trans* isomerization in rhodopsin which reveals that the first step in vision occurs on a 200-fs time scale and is one of the fastest photochemical reactions ever studied.

Rhodopsin ($\lambda_{max}$ ~500 nm) consists of the 11-*cis* retinal prosthetic group (Fig. 1) bound within the protein opsin. Yoshizawa and Wald (*5*) determined that the absorption of light results in the *cis*-to-*trans* isomerization of 11-*cis* retinal to form a red-absorbing photoproduct, bathorhodopsin. Early measurements of the isomerization kinetics


R. W. Schoenlein and C. V. Shank, Lawrence Berkeley Laboratory, University of California, Berkeley, CA 94720.
L. A. Peteanu and R. A. Mathies, Department of Chemistry, University of California, Berkeley, CA 94720.

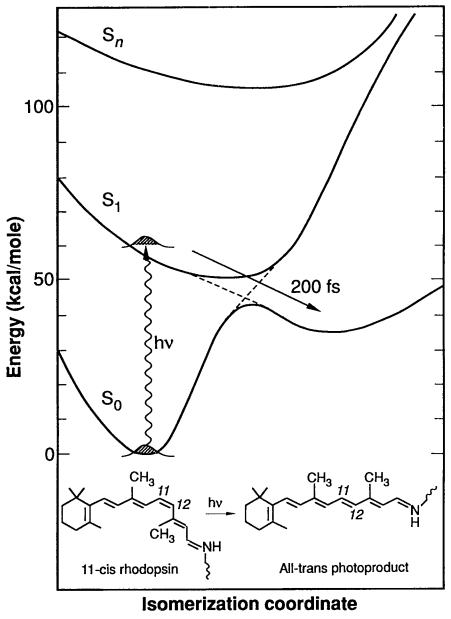


**Fig. 1.** Schematic ground-state and excited-state potential energy surfaces for the 11-*cis* → 11-*trans* isomerization in rhodopsin, adapted from (*14*). The reaction path of the photoisomerization is indicated by the nonadiabatic potential surfaces (broken lines).

by means of transient absorption spectroscopy showed the formation of a photoproduct within the 6-ps pulse duration (*6*). More recently, with lower intensity 25-ps pulses, Shichida *et al.* (*7*) detected a short-lived intermediate, photorhodopsin ($\lambda_{max}$ ~570 nm), which decays to bathorhodopsin ($\lambda_{max}$ ~535 nm) (*8*) in ~40 ps. In addition, studies of rhodopsin with resonance Raman spectroscopy show that the chromophore in the primary photoproduct, trapped at low temperature, has a twisted all-*trans* structure (*9, 10*). Time-resolved Raman studies reveal that at room temperature a similar chromophore structure is formed in less than 30 ps (*11*). Raman intensity analysis, as well as fluorescence quantum yield studies, have suggested that the initial isomerization dynamics occur on a subpicosecond time scale (*12, 13*), and theoretical simulations of the isomerization dynamics are qualitatively consistent with this picture (*14, 15*). However, the time scale for the formation of the primary photoproduct has never been experimentally determined.

The recent development of a blue-green femtosecond laser system (*4*), now makes it possible to directly study the time course of rhodopsin isomerization. The laser system consists of a colliding pulse mode-locked dye laser with a 400-Hz excimer-pumped dye amplifier producing 50-fs pulses at 620 nm with pulse energies of several microjoules. The amplified pulses are used to generate a white-light continuum in an ethylene glycol jet, and the blue-green portion of the continuum is re-amplified to the microjoule level in a second dye amplifier pumped by the same excimer laser. We use a standard pump-probe technique in which a femtosecond pump pulse excites the rhodopsin sample, and the resulting changes in absorption are measured with a probe pulse, which is delayed in time with respect to the pump. The 35-fs pump pulse at 500 nm comes directly from the amplifier. The 10-fs probe pulse is created by splitting off part of the pump and focusing it in an optical fiber to generate a spectrally broadened and chirped pulse. This pulse is then compressed by means of a sequence of gratings and prisms for phase compensation (*16*). The 450- to 580-nm bandwidth of the probe pulses allows us to resolve the spectral dynamics of the rhodopsin molecule following excitation by the narrow-band (~15 nm) pump pulses.

The rhodopsin sample is prepared by isolating rod outer segments from bovine retinas (*10*). The isolated outer segments are purified by ultracentrifugation in a continuous sucrose gradient, lysed with cold water, and pelleted by additional centrifugation. Rhodopsin from 400 retinas is solubilized (5% Ammonyx-LO, 20 mM MOPS, pH 7.4) and then concentrated to an optical density of 15 OD/cm (at 500 nm) using Amicon CF25 centriflo membrane cones. A 3-ml sample was flowed through a 300-μm wire-guided jet at a sufficient velocity to ensure complete replacement of the sample between each pair of pump-probe pulses. The 35-fs pump pulses are focused on the rhodopsin jet to an energy density of ~400 μJ/cm$^2$ (~70-μm spot size). At these pump fluences, only ~10% of the exposed sample is bleached by the pump. The weaker probe pulses are similarly focused on the sample (~30 μJ/cm$^2$). Transient changes in absorption ($\Delta T/T$) are measured with two different techniques. Time-resolved measurements at specific wavelengths are obtained by spectrally filtering the probe pulse (after passing through the sample) and combining differential detection with lock-in amplification. Differential spectral measurements over the entire bandwidth of the 10-fs probe pulse are made with a spectrometer and a dual diode array detector. In all measurements, the maximum signal ($\Delta T/T$) is a few percent, and the linearity is verified in order to avoid saturation effects.

The transient change in absorption is measured at 500, 535, 550, and 570 nm, following excitation of rhodopsin by a 35-fs pulse at 500 nm (Fig. 2). Measurements at 500 nm probe the initial bleach and partial recovery of the ground state absorption of 11-*cis* rhodopsin. At early times, we observe a transient excited-state absorption as evidenced by the negative differential signal ($\Delta T/T<0$) near zero delay. The arrival of the pump pulse induces an absorption at ~500 nm, assigned to the $S_1 \rightarrow S_n$ transition (Fig. 1), which interferes with the ground-state bleach signal. As the wavepacket created in the first excited state moves away from the Franck-Condon region, the excited-state absorption disappears and the full bleach of the rhodopsin absorption is revealed by 125 fs. A rapid partial recovery of the initial bleach at 500 nm is observed, which has a time constant of ~250 fs. The subsequent long-time recovery of the bleach occurs with a time constant of ~8 ps.

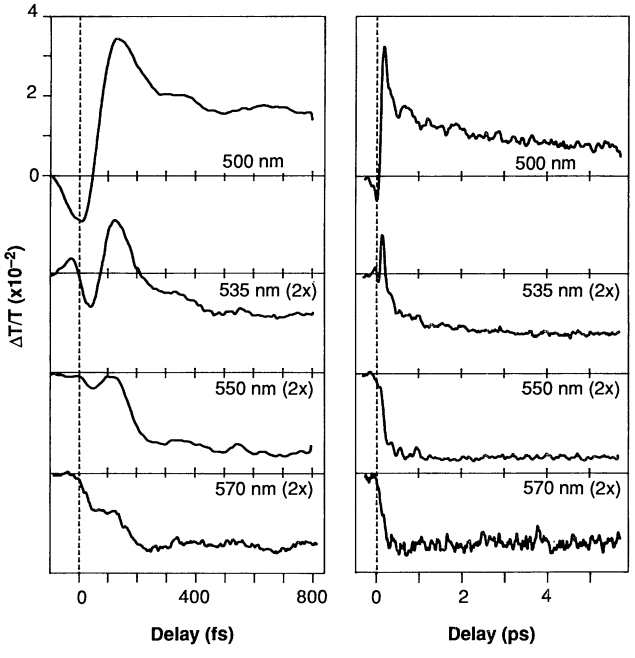


**Fig. 2.** Transient absorption measurements of 11-*cis* rhodopsin at various wavelengths following a 35-fs pump pulse at 500 nm (~10-fs probe).

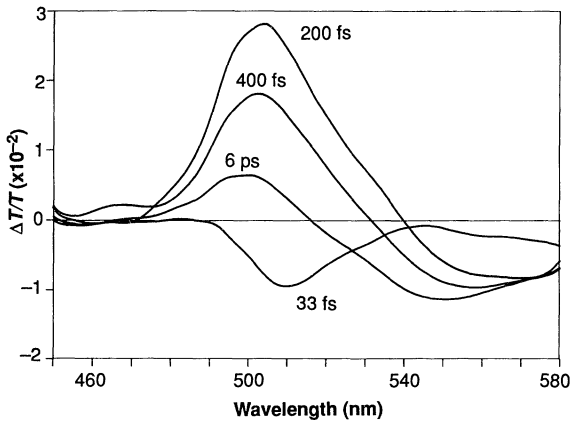


**Fig. 3.** Difference spectra measurements of 11-*cis* rhodopsin at various delays following a 35-fs pump pulse at 500 nm (~10-fs probe).

Transient absorption changes measured at 550 nm and 570 nm reveal the kinetics of photoproduct formation. At 570 nm, near the peak absorption of the photoproduct, we observe a rapidly developing absorption ($\Delta T/T<0$) which reaches a maximum by 200 fs. Beyond 200 fs there is very little change in the absorption, indicating that the photoproduct is formed on this time scale. This conclusion is supported by the rapid appearance of absorption at 550 nm, on the blue side of the photoproduct absorption band. At this wavelength however, there is a ~100-fs delay before the absorption develops. Between 200 fs and 1 ps, the absorption at 550 nm gradually increases, and then remains unchanged out to 6-ps delay.

Measurements at 535 nm, on the red edge of the 11-*cis* rhodopsin absorption band and on the blue edge of the photoproduct absorption, are more complicated. The excited-state ($S_1 \rightarrow S_n$) absorption induced by the pump ($\Delta T/T<0$) is apparent at short times between 0 and 100 fs. This induced absorption does not appear instantaneously as is the case at 500 nm, but is delayed by ~50 fs. The delay is attributed to the dynamics of the excited-state absorption resulting from spreading or motion (or both) of the wavepacket excited on the $S_1$ surface as it leaves the Franck-Condon region. By 100 fs we observe the appearance of the ground-state bleach, and by 200 fs the photoproduct absorption begins to dominate and the signal changes sign. The behavior at longer times (1 to 5 ps) at 535 nm results from a slow recovery of the ground-state absorption (as observed at 500 nm). In addition, we observe oscillatory behavior at all probe wavelengths, though this is particularly evident at 500 nm and at 570 nm (between 0 and 200 fs).

Complementary information about the isomerization kinetics is provided by the differential spectral measurements (Fig. 3). At 33-fs delay, the increase in absorption between 490 and 540 nm results from the excited-state ($S_1 \rightarrow S_n$) transition which dominates the bleach signal at short times. The initial appearance of photoproduct is indicated by the differential absorption observed between 540 and 580 nm. Between 33 fs and 200 fs, the photoproduct absorption increases, and the initial rhodopsin bleach between 470 and 540 nm becomes evident. The filling in of the bleach signal is observed at longer delays, consistent with the time-resolved measurements (Fig. 2). The photoproduct absorption at 570 nm remains unchanged after 200 fs, indicating that the isomerization is complete on this time scale. The blue shift of the isosbestic point (from 540 to 515 nm) with increasing delay is most likely due to vibrational cooling of both the rhodopsin and photoproduct ground states, as well as conformational relaxation. Although we cannot exclude the possibility that some residual excited-state population contributes to the recovery of the bleach at long times, our interpretation is supported by the fact that vibrational cooling and conformational relaxation are known to occur in the related pigment, bacteriorhodopsin, on a similar time scale, ~3 ps (*17*). Differential absorption spectra at 6-ps delay show the residual bleach between 470 and 515 nm and the photoproduct absorption between 515 and 580 nm.

These femtosecond measurements have temporally resolved the isomerization of the 11-*cis* retinal prosthetic group in rhodopsin. The rapid increase in absorption between 540 and 580 nm shows that the all-*trans* photoproduct is formed in only 200 fs. This confirms earlier suggestions that the photosensitivity and high quantum yield of rhodopsin require a rapid non-radiative isomerization (*12, 13*). Furthermore, the non-exponential kinetics observed at 550 nm and 570 nm (Fig. 2) indicate that the isomerization cannot be described by a first-order process. The appearance of the excited-state absorption at ~500 nm at short times is consistent with theoretical models of the electronic structure of the 11-*cis* chromophore in rhodopsin (*14, 18*). The rapid disappearance of this absorption is most likely due to the speed of the torsional motion. The lack of any obvious evidence for stimulated emission from the excited state also indicates that the torsional wavepacket on the excited-state surface rapidly moves out of the Franck-Condon region. In addition, the 100- to 200-fs oscillatory behavior in the time-resolved measurements at 500 nm, as well as at 535, 550, and 570 nm indicates that non-stationary vibrational states are excited by the short pulses (*19*). The vibrational frequency of these oscillations (~135 $cm^{-1}$) is consistent with known low-frequency torsional modes of rhodopsin (*12*), suggesting that excited-state torsional oscillations (*14, 15*) may modulate the appearance of photoproduct. However, impulsive Raman excitation of the rhodopsin ground state can also contribute to coherent vibrational oscillations in these measurements (*20*). Detailed analysis of these oscillations may provide a basis for accurate modeling of the photochemical potential surfaces (*21*).

The difference spectra at long delays are in reasonable agreement with previous measurements made with substantially longer pulses (*7, 22, 23*). Difference spectra at 6 ps delay (Fig. 3) indicate an isosbestic (~515 nm) which is within the range of values previously reported. Although our measurements of the differential absorption maxima (~500 nm and ~550 nm) are slightly shifted from what others have observed, this may be due to measurement uncertainty or the shorter wavelength (500 nm) of the excitation pulses used here, or both. In addition, the signal ratio $\Delta\alpha_{batho}/\Delta\alpha_{rhodopsin} \approx 3$ measured at 40-ps delay (not shown), is consistent with single-photon excitation (*23*). Because we use pulses that are shorter than the ground-state-recovery and photoproduct-formation times, with fluences (~400 $\mu J/cm^2$ or ~0.1 photons absorbed per molecule) that are much lower than previous studies, the possibility of multiphoton photolysis is minimized. Finally, because the time scale of our measurements is faster than the photo→bathorhodopsin transition, we assume that the initial photoproduct is the intermediate, photorhodopsin, identified by Shichida *et al.* (*7*).

In conclusion, we have time-resolved the spectral dynamics of the primary step in vision. Our results indicate that the *cis-trans* isomerization of rhodopsin is essentially complete in only 200 fs. This observation has important implications for the photochemistry of vision. First, 200 fs is faster than typical vibrational dephasing and relaxation times (*19*), suggesting that the photochemistry occurs from a vibrationally coherent system. Indeed, we see indications of

coherent vibrational oscillations which are rapidly damped (at 570 nm) as the photoproduct is formed. The significance of such vibrational coherence in the photochemistry of vision has been discussed in several theoretical studies (*14, 15*). Second, the speed of the isomerization process contradicts the traditional picture of photochemistry which assumes vibrational relaxation in the excited state followed by partitioning to photoproduct and to reactant (*24*). Our results indicate an essentially barrierless transition in the formation of photoproduct, suggesting that the isomerization follows a nonadiabatic potential surface (broken lines in Fig. 1) which reflects the strong coupling between the rhodopsin excited-state and the ground-state of the photoproduct. This presents experimental evidence for a new paradigm for visual photochemistry that may be relevant for a variety of photochemical and photobiological processes.


REFERENCES AND NOTES

1. G. Wald, *Science* **162**, 230 (1968).
2. C. V. Shank, *ibid.* **233**, 1276 (1986).
3. R. A. Mathies, C. H. Brito Cruz, W. T. Pollard, C. V. Shank, *ibid.* **240**, 777 (1988).
4. R. W. Schoenlein, J.-Y. Bigot, M. T. Portella, C. V. Shank, *Appl. Phys. Lett.* **58**, 801 (1991).
5. T. Yoshizawa and G. Wald, *Nature* **197**, 1279 (1963).
6. G. E. Busch, M. L. Applebury, A. A. Lamola, P. M. Rentzepis, *Proc. Natl. Acad. Sci. USA* **69**, 2802 (1972).
7. Y. Shichida, S. Matuoka, T. Yoshizawa, *Photobiochem. Photobiophys.* **7**, 221 (1984).
8. H. Kandori, Y. Shichida, T. Yoshizawa, *Biophys. J.* **56**, 453 (1989).
9. G. Eyring *et al.*, *Biochemistry* **19**, 2410 (1980).
10. I. Palings *et al.*, *ibid.* **26**, 2544 (1987).
11. G. Hayward, W. Carlsen, A. Siegman, L. Stryer, *Science* **211**, 942 (1981).
12. G. R. Loppnow and R. A. Mathies, *Biophys. J.* **54**, 35 (1988).
13. A. G. Doukas *et al.*, *Proc. Natl. Acad. Sci. USA* **81**, 4790 (1984).
14. R. R. Birge and L. M. Hubbard, *J. Am. Chem. Soc.* **102**, 2195 (1980). R. R. Birge, *Annu. Rev. Phys. Chem.* **41**, 683 (1990).
15. R. M. Weiss and A. Warshel, *J. Am. Chem. Soc.* **101**, 6131 (1979).
16. R. L. Fork, C. H. Brito Cruz, P. C. Becker, C. V. Shank, *Opt. Lett.* **12**, 483 (1987).
17. S. J. Doig, P. J. Reid, R. A. Mathies, *J. Phys. Chem.* **95**, 6372 (1991).
18. R. R. Birge, personal communication.
19. H. L. Fragnito, J.-Y. Bigot, P. C. Becker, C. V. Shank, *Chem. Phys. Lett.* **160**, 101 (1989).
20. W. T. Pollard, H. L. Fragnito, J.-Y. Bigot, C. V. Shank, R. A. Mathies, *ibid.* **168**, 239 (1990).
21. W. T. Pollard, S.-Y. Lee, R. A. Mathies, *J. Chem. Phys.* **92**, 4012 (1990).
22. T. G. Monger, R. R. Alfano, R. H. Callender, *Biophys J.* **27**, 105 (1979).
23. J. D. Spalink, A. H. Reynolds, P. M. Rentzepis, W. Sperling, M. L. Applebury, *Proc. Natl. Acad. Sci. U.S.A.* **80**, 1887 (1983).
24. For example see: T. Rosenfeld, B. Honig, M. Ottolenghi, J. Hurley, T. G. Ebrey, *Pure Appl. Chem.* **49**, 341 (1977).


25. Supported by NIH grant EY 02051 (R.M.) and NSF grant CHE 86-15093 (R.M.) and by DOE contract DE-AC03-76SF00098 (C.S.). L.P. acknowledges generous support from NIH postdoctoral training grant T32EY07043.

15 July 1991; accepted 23 August 1991


# Targets for Dioxin: Genes for Plasminogen Activator Inhibitor–2 and Interleukin-1β


THOMAS R. SUTTER, KAREN GUZMAN, KAREN M. DOLD, WILLIAM F. GREENLEE*



**Dioxin (2,3,7,8-tetrachlorodibenzo-*p*-dioxin, TCDD), a widespread environmental contaminant, may elicit its effects by altering gene expression in susceptible cells. Five TCDD-responsive complementary DNA clones were isolated from a human keratinocyte cell line. One of these clones encodes plasminogen activator inhibitor–2, a factor that influences growth and differentiation by regulating proteolysis of the extracellular matrix. Another encodes the cytokine interleukin-1β. Thus, TCDD alters the expression of growth regulatory genes and has effects similar to those of other tumor-promoting agents that affect both inflammation and differentiation.**


TCDD IS AMONG THE MOST TOXIC pollutants known, and it is a prototype for a large class of halogenated aromatic hydrocarbons (*1*). It is carcinogenic (*2*) and teratogenic (*3*) in rodents, but effects of exposure to TCDD in humans are less well understood (*4*). In humans the most common adverse response to TCDD is chloracne (*5*). The pathogenesis of this disorder is characterized by altered patterns of proliferation and differentiation in the epidermis and cutaneous appendages, resulting in interfollicular hyperkeratosis and acanthosis and squamous metaplasia of the epithelial lining of the sebaceous glands, with subsequent hair follicle atrophy (*6*). These effects and others associated with exposure to TCDD in both humans and in other animals are believed to occur through the high-affinity binding of TCDD to the aryl hydrocarbon receptor (AhR) and subsequent changes of gene expression in responsive cells (*1, 7, 8*). The first TCDD-responsive gene to be isolated and the most extensively studied one is cytochrome $P_1$-450 (CYP1A1). Increased transcription of CYP1A1 (P45O1A1) requires accumulation of the TCDD-AhR complex in the nucleus and interaction of the complex with specific DNA response elements (DRE) (*7*).

To elucidate the events occurring in human cells in response to treatment with TCDD, we used differential hybridization to isolate five different TCDD-responsive cDNA clones. Two of these, clones 18 and 142, represent full-length cDNAs (Table 1). One clone was identified as CYP1A1 by cross-hybridization to a CYP1A1 probe (*9*). The kinetics of induction of mRNA for each clone was determined by Northern (RNA) blotting (Fig. 1A) and densitometric (Fig. 1B) analysis. During the first 6 hours of TCDD treatment, the amounts of each of these RNAs increased. Beyond 12 hours of treatment, the response of each clone was variable, but the amounts of these RNAs in TCDD-treated cells were higher than those of untreated cells for at least 48 hours, the longest time point examined (Fig. 1B). The observed variability may reflect regulation of both transcription and RNA stability. Studies of the regulation of cytochrome P-450 by TCDD in rodent liver have shown that the two- to tenfold observed increases in transcription rates do not account for the 25- to 100-fold increases in amounts of mRNA (*10*).


Chemical Industry Institute of Toxicology, Research Triangle Park, NC 27709.

*To whom correspondence should be addressed at Department of Pharmacology and Toxicology, School of Pharmacy and Pharmacal Sciences, Purdue University, West Lafayette, IN 47907.


**Table 1.** Isolation of TCDD-responsive clones. A cDNA library was prepared from RNA isolated from a subclone (c12c2) of the human keratinocyte cell line SCC-12F (*18*) treated for 6 hours with TCDD (10 nM) and CHX (10 μg/ml). The cells were grown until they were confluent in Dulbecco's modified Eagle's medium (DMEM) (1.8 mM $Ca^{2+}$) supplemented with fetal calf serum (FCS) (5%). The medium was then replaced with DMEM containing a low concentration of $Ca^{2+}$ (50 μM) and FCS (1%), and the cells were cultured for 18 to 24 hours. These cells were then treated in DMEM (1.8 mM $Ca^{2+}$) and FCS (1%). A total of 110,000 cDNA clones were screened (*32*) in two rounds (50,000 cDNA clones were screened in screen I). Further analyses of the 142 potential positives identified 16 TCDD-responsive clones, representing five different genes.

| Clone | Isolates* | cDNA size (bp)† | mRNA size (kb)† |
|---|---|---|---|
| CYP1A1 | 4 (0) | 2050 | 3.0 |
| 18 | 5 (4) | 2100 | 1.9 |
| 1 | 5 (2) | 1550 | 5.1 |
| 141 | 1 (0) | 1500 | 5.2 |
| 142 | 1 (0) | 1400 | 1.5 |

*Indicates the number of times a related cDNA clone was independently isolated. The value in parentheses indicates the number isolated in Screen I only. †After we performed gel electrophoresis, sizes were determined by comparison with DNA or RNA standards (Gibco-BRL), as appropriate.